Three-Dimensional Structure of Cholera Toxin Penetrating a Lipid Membrane

HANS O. RIBI, DAVID S. LUDWIG, K. LYNNE MERCER, GARY K. SCHOOLNIK, ROGER D. KORNBERG

Two-dimensional crystals of cholera toxin bound to receptors in a lipid membrane give diffraction extending to 15 Å resolution. Three-dimensional structure determination reveals a ring of five B subunits on the membrane surface, with one-third of the A subunit occupying the center of the ring. The remaining mass of the A subunit appears to penetrate the hydrophobic interior of the membrane. Cleavage of a disulfide bond in the A subunit, which activates the toxin, causes a major conformational change, with the A subunit mostly exiting from the B ring.

MANY POLYPEPTIDE TOXINS AND GLYCOPROTEIN HORMONES are composed of two types of chain, one (B) which binds a cell surface receptor, and a second (A) which traverses the cell membrane and exerts a biological effect (*1–4*). Cholera toxin is a particularly well-studied example, with a B subunit (12 kilodaltons) that binds the ganglioside GM1, and an A subunit (27 kD), part of which penetrates the cell and catalyzes the ADP-ribosylation (ADP, adenosine diphosphate) of the stimulatory G component of adenylate cyclase (*5–10*). From evidence for a stoichiometry of AB_5 or AB_6, it has been proposed that the A subunit lies on the central axis of a ring of B subunits (*7, 11–13*). The A subunit is divided by proteolytic cleavage and chemical reduction into two fragments, A1 (22 kD), which has catalytic activity, and A2 (5 kD), presumed to mediate the interaction of A1 with B subunits. Both cleavage and reduction are required for catalytic activity (*14*). The A1 fragment has been suggested to traverse a cell membrane either through a hydrophilic pore formed by B subunits extending across the lipid bilayer (*6, 15*), or by direct interaction with the hydrophobic interior of the bilayer (*16*).

We have investigated the structure and mechanism of membrane penetration of cholera toxin by the lipid layer crystallization technique (*17–20*). Elsewhere we described crystals of oligomers of B subunits formed on lipid layers containing GM1 (*21*). Imaging in projection at 15 Å resolution by electron crystallography revealed rings of five protein densities lying flat on the membrane surface. Here we describe crystals of the complete toxin and its activated (chemically reduced) form, and compare the structures with that of the B oligomer by the calculation of difference maps in projection at 15 Å resolution and by full three-dimensional structure determination. The results reveal an arrangement of B subunits in the complete toxin nearly identical to that in the B oligomer, consistent with preliminary x-ray studies (*11*) and electron microscopy at 30 Å resolution (*22*). The results further establish the location of the A subunit and show how the structure of the toxin is altered by activation.

Two-dimensional crystals of cholera toxin. The lipid layer crystallization technique entails binding of a macromolecule to a lipid-ligand in mono- or multilayers. Oriented binding, high protein concentration, and lateral diffusion of lipids facilitate the formation of two-dimensional crystals amenable to structure determination by electron microscopy and image processing. The technique is appropriate for studies of cholera toxin, with GM1 as lipid-ligand, since the toxin is revealed in a biologically relevant context, bound to receptors in a lipid membrane. Our results were obtained with dioleoyl-phosphatidylcholine or -phosphatidylethanolamine mixed with 10 percent (molar) GM1, a concentration sufficient to bind almost all the B subunits (*23, 24*) in the arrays described below.

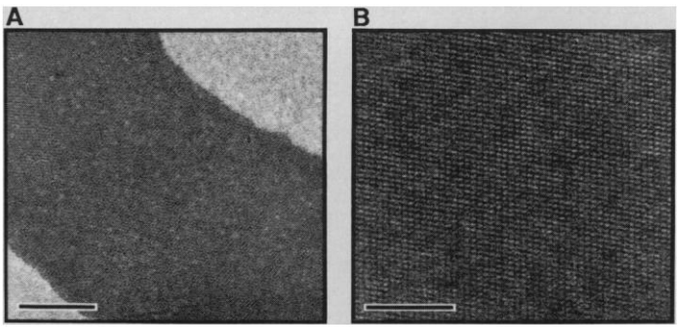

Fig. 1. Electron micrographs of cholera toxin crystals on layers of GM1 and dioleoyl-phosphatidylethanolamine. (**A**) Image of a crystalline region (darkly staining area) at low magnification (scale bar corresponding to 1500 Å) and a tilt angle of 15°. (**B**) Image at higher magnification (scale bar corresponding to 900 Å) and tilt angle of 51°. Lipid solution [1 μl of chloroform and hexane, 1:1 by volume, containing GM1 (Supelco) at 0.1 mg/ml and dioleoyl-phosphatidylethanolamine (Avanti Polar Lipids) at 0.4 mg/ml] was applied to the surface of 50 μl of protein solution [cholera toxin at 250 μg/ml (Sigma) in 0.2*M* sodium borate, *p*H 8.2, or 0.01*M* tris-HCl, *p*H 7.2, and 0.15*M* NaCl] in a Teflon well (5 by 10 mm, 1 mm deep). Alternatively, protein solution (10 μl; 1 mg/ml) was injected beneath preformed lipid layers, with essentially the same results. After incubation in a humid atmosphere at room temperature, carbon-coated electron microscope grids were brought in contact with the film in the trough, withdrawn, washed with a drop of water or buffer solution, and stained with 1 percent uranyl acetate. The cholera toxin was analyzed in SDS-polyacrylamide gels, before and after treatment with 2-mercaptoethanol. Less than 10 percent of the material was in a reduced state before mercaptoethanol treatment, and 95 percent or more was proteolytically cleaved (releasing free A1 upon reduction).

H. O. Ribi, K. L. Mercer, and R. D. Kornberg are in the Department of Cell Biology, D. S. Ludwig is in the Departments of Medicine and Medical Microbiology, and G. K. Schoolnik is in the Departments of Medicine and Medical Microbiology, Division of Geographic Medicine, and the Howard Hughes Medical Institute at the Stanford University School of Medicine, Stanford, CA 94305.

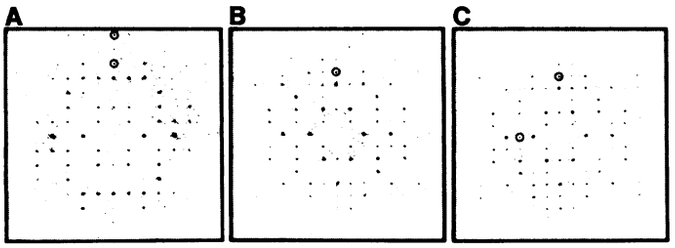

Fig. 2. Optical diffraction patterns from images of (untilted) rectangular lattices of (**A**) B oligomer, (**B**) complete toxin, and (**C**) toxin reduced by injection of dithiothreitol (5 μl of a 0.1*M* solution in 0.2*M* sodium borate, *p*H 8.2) beneath the surface of crystals grown for 2 days and then incubated for another day. Circles identify reflections forbidden by *pgg* symmetry. The B oligomer, affinity-purified from filtrates of *Vibrio cholerae* strain 569B (*35*) was from the Institute Merieux (Marcy, France) or from Sigma. Crystals were grown as described in Fig. 1.

Lipid layers were formed by spreading lipids from a volatile solvent on the surface of 50 μl of an aqueous solution in a Teflon well. The amount of lipid was in excess of that needed to form a single monolayer on the well, compensating for losses around the edges and losses due to vesicle formation during spreading, and ensuring the presence of a film near its maximum spreading pressure. The yield of protein crystals was lower with films maintained below maximum spreading pressure, presumably because proteins unfold and compete with lipids for area at the air-water interface (*18*).

Cholera toxin was either present in the aqueous solution before the application of lipids, or it was injected beneath a preformed lipid film to avoid denaturation at the air-water interface. Areas of the lipid film and associated protein crystals were recovered after an incubation period by placement of a carbon-coated electron microscope grid on the film, withdrawal of the grid, and then negative staining. The hydrophobic layer of carbon on the grid generally retained the film with the hydrocarbon chains of the lipids abutting the carbon. Films oriented in this way, with protein exposed on the surface, were well contrasted by stain, whereas those that had been flipped or folded during transfer showed little contrast.

Cholera toxin formed arrays up to 100 μm across with a high degree of order in some areas (Fig. 1) during 6 to 64 hours incubation at 23° to 30°C and under physiologic conditions of *p*H and ionic strength. Array formation required GM1, indicating the involvement of specific protein-binding in the process. Optical diffraction from electron micrographs revealed both rectangular (Fig. 2, A and B) and hexagonal crystal lattices, isomorphous with those previously obtained for the B oligomer (*21*). Treatment of cholera toxin crystals with dithiothreitol, to cleave the disulfide bond in the A subunit and release active A1 fragment (*25, 26*), did not affect the crystal lattices but did alter the amplitudes of many reflections in the diffraction pattern (Fig. 2C), indicative of a change in molecular structure.

Projected structures and difference maps. Since rectangular lattices of the B subunit are truly crystalline (*21*), whereas hexagonal lattices are partially disordered or liquid crystalline, we have used only rectangular lattices of the B oligomer, complete toxin, and activated toxin to derive structural information. In all three cases, diffraction extended to a ninth-order reflection (1/15 Å), the approximate limit of resolution for crystals in negative stain. Several images of each form of the toxin were processed by standard methods (*27*) (Table 1). Imposition of *p*2 projection symmetry was justified by (i) the appearance, in noise-filtered images, of pairs of pentagonally shaped protein densities centered on a twofold axis perpendicular to the plane of the protein lattice; and (ii) average deviations from centrosymmetric phases, after origin refinement, of 13.1° or less in all cases. Average Fourier transforms were used to calculate projected structures (Fig. 3, A, B, and D).

One unit cell of each form of the toxin (dimensions a = 120 Å, b = 131 Å, γ = 90°) contained four pentagonally shaped protein densities. In the case of the B oligomer, this density was concentrated in a ring of five peaks around a central channel (Fig. 3A). Identification of the peaks with individual subunits was supported by the results of three-dimensional structure determination described below. In the complete toxin, the size of the pentagonal region was the same, but the central channel was filled with additional density and the five peaks were obscured (Fig. 3B). Finally, the structure of the activated toxin appeared intermediate between those of the B oligomer and the complete toxin (Fig. 3D).

The location of additional density in the complete and activated toxin was revealed by the calculation of difference maps. Average Fourier components determined for the B oligomer were subtracted from those of the complete and activated toxins. Difference density distributions were obtained with four peaks in the unit cell which, when superimposed on the B oligomer, lay directly over the central channel (Fig. 3, C and E). The difference peaks were highly significant, inasmuch as the variation in density in the peak regions among the individual images analyzed was small: the mean density (in arbitrary units, averaged over the four peak regions in the unit cell) was -25 ± 8 ($x \pm$ SD) for images of the B oligomer, 45 ± 9 for the complete toxin, and 25 ± 8 for the activated toxin. The location of the difference peaks indicated that the A subunit occupied the central channel, but there was a quantitative discrepancy. The mean density in the central region of the complete toxin was

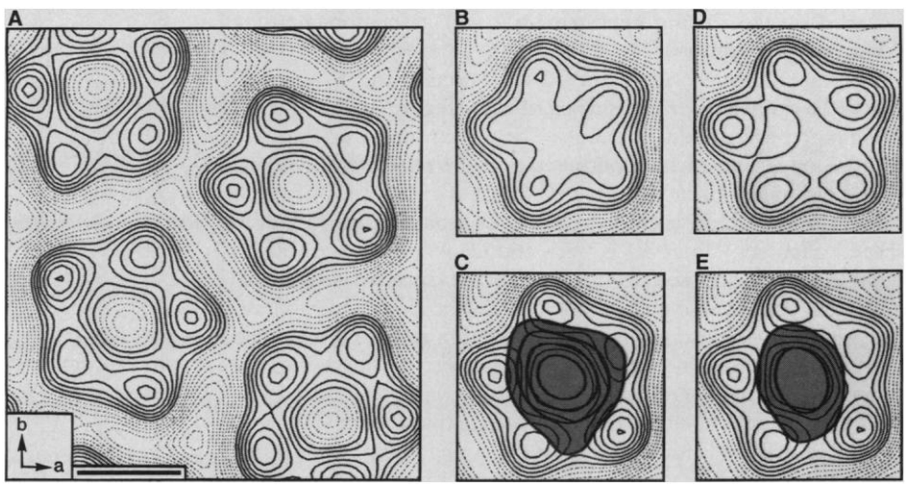

Fig. 3. Projected structures of (**A**) B oligomer, (**B**) complete toxin, (**D**) activated toxin, and difference maps (shaded, with bold contours) of (**C**) complete toxin minus B oligomer, superimposed on the projected structure of the B oligomer, and (**E**) activated toxin minus B oligomer, superimposed on the projected structure of the B oligomer. A complete unit cell, containing four pentagonally shaped regions of protein density, is shown in (A), and one pentagonal region or corresponding difference peak is shown in (B) to (E). The series of solid and dashed contour lines represent increasing levels of protein density and stain accumulation, respectively. Arrows indicate directions of lattice vectors. Scale bar corresponds to 30 Å.

Table 1. Image processing of electron micrographs.

Structures	B oligomer	Complete toxin	Activated toxin
	Projected		
Images averaged (No.)	6	6	4
Average phase error/image	11.5°	12.5°	13.1°
Fourier terms (No.)	60	50	40
Symmetry imposed	*p*2	*p*2	*p*2
	Three-dimensional		
Images (No.)	26	19	10
Average phase error/image	19	22.9	21.2
Fourier terms (No.)	207	156	142
Independent lattice lines (No.)	52	39	39
Range of tilt angles	0–52°	0–51°	0–51°
Symmetry imposed	*p*21	*p*21	*p*21

nearly identical with that of the peaks identified with the B subunits, whereas the mass of an A subunit is more than twice that of a B subunit. Approximately 60 percent of the A subunit was unaccounted for in the structure of the complete toxin. An explanation for this discrepancy, which we favor in light of arguments below, is that part of the A subunit is embedded in the hydrophobic interior of the lipid membrane, inaccessible to the negative stain outlining the structure. An alternative explanation would be that part of the A subunit is located above the channel, off the central axis, in any one of five equivalent positions, and makes little contribution to the computed structure, due to averaging over many molecules in a crystal.

The change in density in the central region that occurred upon activation of the toxin by chemical reduction, together with the effect of reduction on the A subunit, further indicated a central location of the A subunit. The central density in the activated toxin was approximately half of that identified with a B subunit, and corresponded with the mass of the A2 fragment. The central density could, however, have been due to a vestige of the A1 fragment, and a definitive assignment must await the isolation and structure determination of an A2-B complex.

Three-dimensional structures. The conclusions drawn from projection maps were confirmed and extended by three-dimensional structure determination. Data from images of tilted crystals extended to resolutions of about 20 Å for the B oligomer and the complete toxin, and about 25 Å for the activated toxin (Fig. 4 and Table 1). The specimens analyzed clearly contained a single layer of protein molecules, since the diffraction maxima were sharp over a range of tilt angles about various tilt axes and since views of edges of the crystals showed only one layer. Regions of crystals where overlap occurred due to folding appeared thick and gave superimposing diffraction patterns.

The three-dimensional density distribution of the B oligomer revealed a ring of five barrel-shaped objects (Fig. 5, A to C), which we interpret as individual subunits. The objects measured about 25 by 40 Å on average, when contoured near the zero level. An object of these dimensions would have 95 percent of the mass of the B subunit (density 1.31 g/cm^3). The ring of subunits formed a disk-shaped oligomer, about 40 Å thick and 60 Å in diameter, bound with one face apposed to the membrane surface, presumably through a GM1-binding site at the ends of the elongated subunits. The variable orientation of the subunits within a single B oligomer, either standing on end or tilted with respect to the membrane surface, may not be significant at the resolution of this analysis.

The three-dimensional structure of the complete toxin (Fig. 5, D to F) was nearly identical to that of the B oligomer, except in the central channel, where there was extra density in the complete toxin. The correspondence of external features in the two structures indicated that the arrangement of B subunits was the same, so the extra density in the complete toxin must be attributed to the A subunit. The strength of the extra density was comparable to that elsewhere in the structure, but this density only partially filled the central channel (Fig. 5F), giving the toxin an indented appearance on the face opposite the membrane surface (Fig. 5D). The volume of the extra density represented less than half of that expected from the mass of the A subunit, in agreement with the analysis of the density in projection, described above. The question of whether the missing density lay above or beneath the rest of the structure was addressed on the basis of the three-dimensional data. The density seen in the channel did not reach the upper surface, and so would most plausibly extend beneath the structure. That is, most of the A subunit, about 16 kD, appeared to reside within the hydrophobic interior of the lipid membrane, inaccessible to the negative stain outlining the structure. A sphere of this mass (and density 1.31 g/cm^3) would be about 35 Å in diameter, and so would nearly span a lipid bilayer membrane.

Upon activation of the toxin by chemical reduction, the density in the central channel largely disappeared, leaving a residual mass of at most 5 kD (Fig. 5, G to I), in agreement with the projected structures above. The rest of the structure was virtually identical to

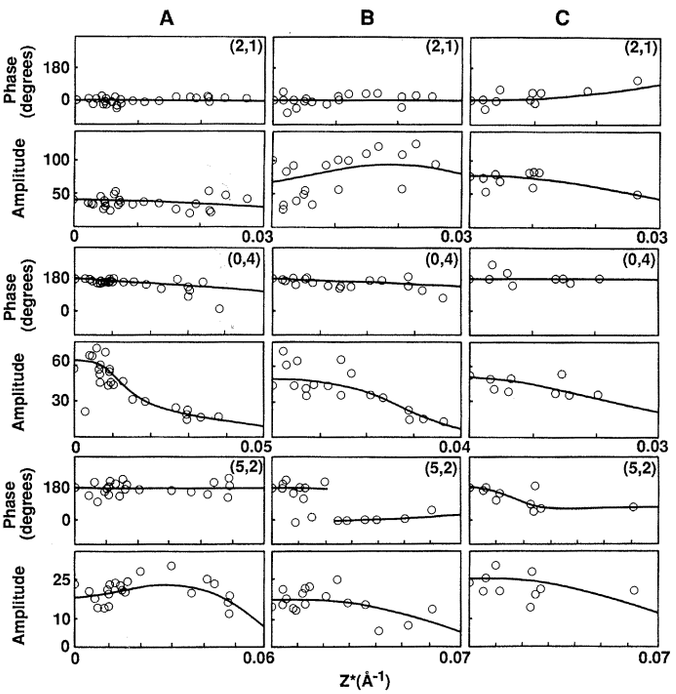

Fig. 4. Phase and amplitude variation along the (2,1), (0,4), and (5,2) lattice lines of (**A**) the B oligomer, (**B**) complete toxin, and (**C**) activated toxin crystals. Images were recorded at 100 kV at a magnification of 36,000 with a Philips EM400 electron microscope (underfocused 300 to 8000 Å), with minimal electron doses (10 to 15 electron/Å^2 for each image). Care was taken to record the orientation of each grid with respect to the electron beam so that the individual data sets could be properly merged. Images were scanned with a Perkin-Elmer densitometer, with a step and sampling size of 20 μm. Data sets, combined in the three-dimensional analysis by standard methods (*29*), gave average phase errors upon origin refinement of less than 30° (Table 1). Tilt axes were calculated from distortions of the reciprocal lattices, and tilt angles were taken from goniometer readings. Average data from untilted specimens served as initial sets for refinement of data from tilted specimens (according to the two-sided plane group *p*21), which was carried out with a comparison range in Z^* of 0.0083 Å^{-1}. Terms along the (0,0) lattice lines were not included. Continuous curves were fitted to the experimental points along each lattice line and the curves were then sampled (*36*) at intervals of 0.01 Å^{-1}.

that of the B oligomer. The residual density was clearly located near the base of the channel, but its precise distribution was not well determined at the resolution of this analysis. We conclude that upon activation, the A1 fragment dissociates from the central channel and either remains loosely in contact with the rest of the structure or diffuses away. The B oligomer and possibly the A2 fragment are left behind, bound to the membrane surface, essentially unaffected by the movement of A1.

Two-sided plane group symmetry $p21$ (space group $P2$) was assumed in the three-dimensional analysis because it allowed the structures of the two pairs of molecules in the unit cell to be independently determined. The similarities between the pairs of molecules provided a measure of the quality of the density maps and permitted the occurrence of other symmetries to be objectively assessed. The possible existence of the space group symmetries $P22_12_1$ and $P2_12_12_1$ was suggested by apparent *pgg* symmetry in projection. In both space groups, the two pairs of molecules in the unit cell would be oppositely oriented with respect to the membrane surface, one pair facing the surface and the other facing the aqueous solution. This was not the case in our density maps of the complete and activated toxins, as shown by sections perpendicular to the membrane surface through the centers of the molecules. Sections of the complete toxin (Fig. 6) contained a central peak of density due to the A subunit, with a trough above and with additional lobes of density due to B subunits on either side. (The lobes of density did not extend to the membrane surface because a section through the center of the molecule does not pass through the centers of two B subunits.) The numerical values of the map in the peak, trough, and lobes of density indicated that these features of the map were highly significant. These features define the orientation of a molecule with respect to the membrane surface, and the orientations of the two pairs of molecules in the unit cell were identical. This conclusion could be in error if there were a gross staining artifact, causing oppositely oriented molecules to appear the same. Such an artifact seems unlikely, since the features defining the orientation were among the strongest in the map. Final proof awaits studies at higher resolution or with unstained specimens.

There is no conflict between the apparent *pgg* symmetry of the data in projection and the lack of $P22_12_1$ or $P2_12_12_1$ symmetry in three dimensions. The A subunit appeared centrally located and the

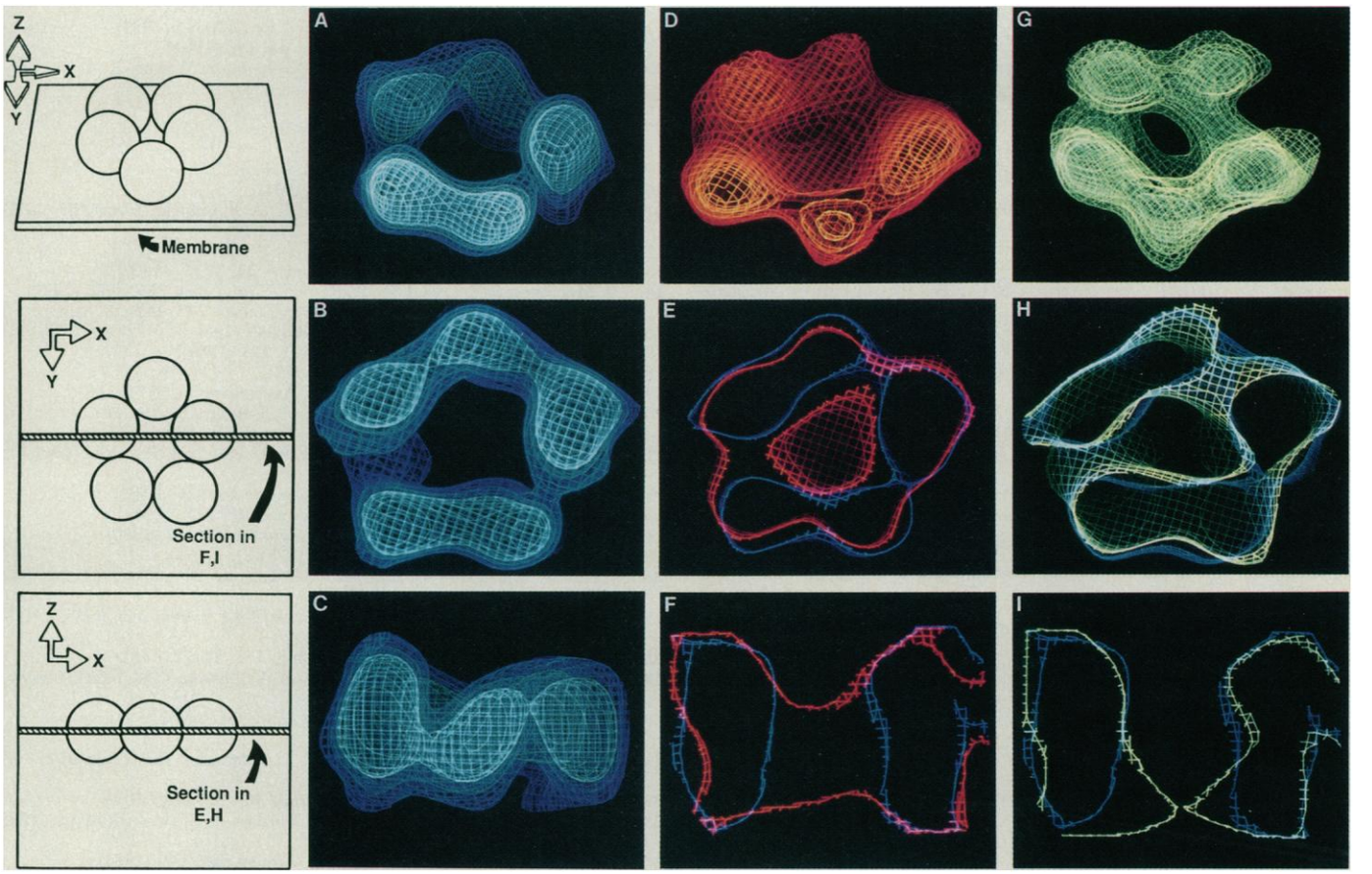

Fig. 5. Three-dimensional structures of the B oligomer (blue), complete toxin (orange-yellow), and activated toxin (green). The schematic drawings of the B oligomer at the left illustrate the direction of view in each row, which is at 45° to the membrane surface in the first row, perpendicular to (down onto) the membrane surface in the second row, and parallel to (in the plane of) the membrane surface (directly below the structure) in the third row. (**A**, **B**, and **C**) The full density distribution of the B oligomer. (**D** and **G**) The full density distribution of the complete toxin and activated toxin, respectively. (**E** and **F**) The structures of the B oligomer and complete toxin are superimposed. (**H** and **I**) The structures of the B oligomer and activated toxin are superimposed. Panels E and H display the density in sections 6 and 20 Å thick through the structure, respectively, depicted as a cross-hatched zone in the schematic at the lower left. Panels F and I display the density in a 2 Å thick section, cross-hatched in the schematic at center left. In panels A to D and G, three contour levels are shown, in different shades of blue, orange-yellow, and green, with the outermost (lowest level) contour enclosing a volume about 95 percent of that expected from the mass of the B oligomer (see text). In panels E and H, only the outermost contours are shown. In panels F and I, a contour level slightly different from the outermost one in the other panels was used, such that the entire mass of the B oligomer is accounted for by the enclosed volume. At each contour level, lines were drawn and displayed at 2 Å intervals, with the use of FRODO version 6.1 (Rice University) and an Evans and Sutherland color graphics system. Contours due to noise between molecules, unconnected with the rest of the density distribution and at the level of noise (zero contour level), were eliminated by masking.

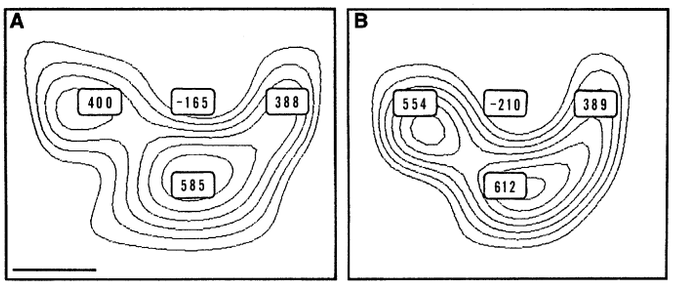

Fig. 6. Contour maps of sections parallel to the (*X, Z*) plane (see schematic drawings in Fig. 5) through the centers of two complete toxin molecules, one from each pair in the unit cell. The membrane surface is located at the bottom of the sections. The numerical values give the densities at the centers of the boxes near the peaks, lobes, and troughs (positive and negative numbers indicating regions of protein and negative stain, respectively). Scale bar corresponds to 15 Å.

B subunits were barrel-shaped at the resolution of our analysis, and therefore the orientations of the subunits were not readily discerned in projection. There were, in fact, deviations from *pgg* projection symmetry (for example, the reflections circled in Fig. 2, which showed significant amplitudes and low phase residuals in computed transforms, are forbidden by *pgg* symmetry). Such deviations should become more significant at higher resolution.

Mechanism of membrane penetration. Two proposals have been put forward for the mechanism of membrane penetration by cholera toxin. The first is that B subunits unfold and extend across the membrane, forming a hydrophilic pore through which the A1 fragment can pass (*6*). The second proposal is that only the A1 fragment traverses the membrane (*16*). The data and interpretations presented here argue against the first and in favor of the second proposal. Virtually the entire mass of the B subunit can be accounted for on the surface of the membrane. There is no hint of a hydrophilic pore in the membrane, which would appear as an extension of the central channel of the B oligomer into the region beneath the subunits in Fig. 5, C, F, and I. Rather, the A1 fragment alone appears to penetrate the membrane.

Our conclusions are in keeping with results obtained by other methods. A photoreactive group at position 12 of a hydrocarbon chain in a phospho- or glycolipid was found to label only the A1 fragment of toxin bound to GM1 in a membrane (*16, 28*). Laser light scattering curves have been interpreted in terms of a model in which B subunits adsorb and remain on the surface of a lipid bilayer, while the A1 fragment is incorporated in the hydrophobic interior (*13*). Although these approaches have given evidence for the membrane penetration of the A1 fragment, they are equivocal regarding the role of reduction in the process, with one study showing a requirement (*28*) for reduction and other studies not revealing an effect (*13, 16*). Our results indicate two stages of membrane penetration, the first occurring before reduction and the second after.

There are at least two ways in which membrane penetration by the A1 fragment may be assisted by B subunits. First, the A1 fragment might be driven into a membrane by the binding of all five sites on the B oligomer to GM1. Second, the pentavalent interaction of the B oligomer with GM1 (*13, 24*) might perturb the close packing of lipids and thereby facilitate the entry of the A1 fragment into the hydrophobic interior of the membrane. Specifically, if five GM1 molecules are constrained at the positions of the subunits in a B oligomer (Fig. 3A), and if the diameters of GM1 and phospholipid molecules are 12 and 10 Å, respectively (*29, 30*), then the maximum number of phospholipids that can occupy the area beneath the oligomer is about 25 percent less than in an unperturbed phospholipid monolayer. This reduction in lipid packing density may account for an increase in permeability of lipid membranes to small, hydrophilic molecules that occur upon binding of the B oligomer (*15, 31*). The effects mentioned here, perturbation of lipid packing and membrane penetration driven by GM1-binding, may well explain the capacity of the A1 fragment to enter the hydrophobic interior of a membrane.

Our study can be extended to higher resolution by electron microscopy of unstained specimens, either in glucose or in ice (*32, 33*). Particularly, it should be possible to determine the distribution of protein in the interior of the membrane (*34*), confirm the location of the A1 fragment within the hydrophobic region, and learn more about the structural changes associated with activation by reduction.

REFERENCES AND NOTES

1. D. M. Gill, in *Bacterial Toxins and Cell Membranes,* J. Jeljaszewics and T. Wadstrom, Eds. (Academic Press, New York, 1978), pp. 291–332.
2. S. van Heyningen, in *Molecular Action of Toxins and Viruses,* P. Cohen and S. van Heyningen, Eds. (Elsevier, New York, 1982), pp. 169–190.
3. L. Eidels, R. L. Proia, D. A. Hart, *Microbiol. Rev.* **47**, 596 (1983).
4. J. L. Middlebrook and R. B. Dorland, *ibid.* **48**, 199 (1984).
5. R. A. Finkelstein, M. Boesman, S. H. Neoh, M. K. LaRue, R. Delaney, *J. Immunol.* **113**, 145 (1974).
6. D. M. Gill, *Biochemistry* **15**, 1242 (1976).
7. ———, *Adv. Cyclic Nucleotide Res.* **8**, 85 (1977).
8. C.-Y. Lai, *J. Biol. Chem.* **252**, 7249 (1977).
9. A. Kurosky, D. E. Markel, J. W. Peterson, *ibid.*, p. 7257.
10. J. Holmgren, *Nature (London)* **292**, 413 (1981).
11. P. B. Sigler, M. E. Druyan, H. C. Kiefer, R. A. Finkelstein, *Science* **197**, 1277 (1977).
12. C.-Y. Lai, *CRC Crit. Rev. Biochem.* **9** (no. 3), 171 (1980).
13. J. D. Dwyer and V. A. Bloomfield, *Biochemistry* **21**, 3227 (1982).
14. J. J. Mekalanos, R. J. Collier, W. R. Romig, *J. Biol. Chem.* **254**, 3855 (1979).
15. M. T. Tosteson and D. C. Tosteson, *Nature (London)* **275**, 142 (1978).
16. B. J. Wisnieski and J. S. Bramhall, *ibid.* **289**, 319 (1981).
17. E. E. Uzgiris and R. D. Kornberg, *ibid.* **301**, 125 (1983).
18. H. O. Ribi, thesis, Stanford University (1987).
19. H. O. Ribi, P. Reichard, R. D. Kornberg, *Biochemistry* **26**, 7974 (1987).
20. R. D. Kornberg and H. O. Ribi, in *Protein Structure, Folding, and Design,* D. Oxender, Ed. (Liss, New York, 1987), vol. 2, pp. 175–186.
21. D. S. Ludwig, H. O. Ribi, G. K. Schoolnik, R. D. Kornberg, *Proc. Natl. Acad. Sci. U.S.A.* **83**, 8585 (1986).
22. R. A. Reed, J. Mattai, G. G. Shipley, *Biochemistry* **26**, 824 (1987).
23. P. H. Fishman, J. Moss, J. C. Osborne, Jr., *ibid.* **17**, 711 (1978).
24. P. H. Fishman and E. E. Atikkan, *J. Membrane Biol.* **54**, 51 (1980).
25. J. Sattler *et al., Eur. J. Biochem.* **57**, 309 (1975).
26. M. Tomasi, A. Battistini, C. Ausiello, L. G. Roda, G. D'Agnolo, *FEBS Lett.* **94**, 253 (1978).
27. L. A. Amos, R. Henderson, P. N. T. Unwin, *Prog. Biophys. Mol. Biol.* **39**, 183 (1982).
28. M. Tomasi and C. Montecucco, *J. Biol. Chem.* **256**, 11177 (1981).
29. T. E. Thompson, M. Allietta, R. E. Brown, M. L. Johnson, T. W. Tillack, *Biochim. Biophys. Acta* **817**, 229 (1985).
30. G. L. Gaines, Jr., in *Insoluble Monolayers at Liquid-Gas Interfaces,* I. Prigogine, Ed. (Wiley, New York, 1966).
31. J. Moss, R. L. Richards, C. R. Alving, P. H. Fishman, *J. Biol. Chem.* **252**, 797 (1977).
32. K. A. Taylor and R. M. Glaeser, *J. Ultrastruct. Res.* **55**, 448 (1976).
33. J. Dubochet, J. Lepault, R. Freeman, J. A. Berriman, J.-C. Homo, *J. Microsc.* **128**, 219 (1982).
34. P. N. T. Unwin and P. D. Ennis, *Nature (London)* **307**, 609 (1984).
35. J. L. Tayot, J. Holmgren, L. Svennerholm, M. Lindblad, M. Tardy, *Eur. J. Biochem.* **113**, 249 (1981).
36. D. A. Agard, *J. Mol. Biol.* **167**, 849 (1983).
37. We thank Drs. P. N. T. Unwin, C. W. Akey, R. A. Milligan, and R. O. Fox for discussions and suggestions and the Institute Merieux (Marcy, France) for a generous gift of B oligomer. Supported by NIH Cellular and Molecular Biology Training grant GM07276-12 (H.O.R.), by NIGMS grant GM07365 (D.S.L.) from the Medical Scientist Training Program, and by NIH grants AI21144 and GM30387 (R.D.K.).

7 August 1987; accepted 29 January 1988